Available online at www.sciencedirect.com

ScienceDirect

www.elsevier.com/locate/jes

JES JOURNAL OF ENVIRONMENTAL SCIENCES

www.jesc.ac.cn

Research Article

Concentrations and light absorption properties of $PM_{2.5}$ organic and black carbon based on online measurements in Lanzhou, China

Pengfei Chen[1,2], *Shichang Kang*[1,2,#,*], *Qinyi Gan*[3], *Ye Yu*[4], *Xianlei Yuan*[5], *Yajun Liu*[1], *Lekhendra Tripathee*[1], *Xiaoxiang Wang*[1], *Chaoliu Li*[1,2]

[1] *State Key Laboratory of Cryospheric Science, Northwest Institute of Eco-Environment and Resources, Chinese Academy of Sciences (CAS), Lanzhou 730000, China*
[2] *University of Chinese Academy of Sciences, Beijing 100049, China*
[3] *College of Earth and Environmental Sciences, Lanzhou University, Lanzhou 730000, China*
[4] *Key Laboratory of Land Surface Process and Climate Change in Cold and Arid Regions, Northwest Institute of Eco-Environment and Resources, CAS, Lanzhou 730000, China*
[5] *Xinjiang Bayingolin Mongolian Autonomous Prefecture Meteorological Bureau, Korla 841000, China*

ARTICLE INFO

Article history:
Received 9 December 2021
Revised 21 April 2022
Accepted 2 August 2022
Available online 19 August 2022

Keywords:
Black carbon
Brown carbon
Light absorption
Source
Lanzhou

ABSTRACT

To elucidate the variations in mass concentrations of organic carbon (OC) and black carbon (BC) in $PM_{2.5}$ and their light absorption characteristics in Lanzhou, we conducted one-year online measurements by using a newly developed total carbon analyzer (TCA08) coupled with an aethalometer (AE33) from July 2018 to July 2019. The mean OC and BC concentrations were 6.4 ± 4.4 and 2.0 ± 1.3 μg/m^3, respectively. Clear seasonal variations were observed for both components, with winter having the highest concentrations, followed by autumn, spring, and summer. The diurnal variations of OC and BC concentrations were similar throughout the year, with daily two peaks occurring in the morning and evening, respectively. A relatively low OC/BC ratio (3.3 ± 1.2, n = 345) were observed, indicating that fossil fuel combustion was the primary source of the carbonaceous components. This is further substantiated by relatively low biomass burning contribution ($f_{biomass}$: 27.1% ± 11.3%) to BC using aethalometer based measurement though $f_{biomass}$ value which increased significantly in winter (41.6% ± 5.7%). We estimated a considerable brown carbon (BrC) contribution to the total absorption coefficient (b_{abs}) at 370 nm (yearly average of 30.8% ± 11.1%), with a winter maximum of 44.2% ± 4.1% and a summer minimum of 19.2% ± 4.2%. Calculation of the wavelength dependence of total b_{abs} revealed an annual mean $AAE_{370\text{-}520}$ value of 4.2 ± 0.5, with slightly higher values in spring and winter. The mass absorption cross-section of BrC also exhibited higher values in winter, with an annual mean of 5.4 ± 1.9 m^2/g, reflecting the impact of emissions from increased biomass burning on BrC concentrations.

* Corresponding author.
E-mail: shichang.kang@lzb.ac.cn (S. Kang).
Shichang Kang will handle correspondence at all stages of refereeing and publication, also post-publication.

https://doi.org/10.1016/j.jes.2022.08.007
1001-0742/

Introduction

Carbonaceous aerosols (CAs), constituting the main component of particulate matter in urban atmospheres, have caused considerable concern because of their large but poorly constrained climate forcing effects and their adverse effects on human health (Bond et al., 2013; Kang et al., 2019; Lelieveld et al., 2015; Li et al., 2020). Organic carbon (OC) and black carbon (BC) in the atmosphere are major components of CAs. OC and BC are responsible for most of the light absorption properties of CAs. BC mainly absorbs solar radiation in the visible and infrared wavelengths (Bond and Bergstrom, 2006; Bond et al., 2013; Hodnebrog et al., 2014), whereas brown carbon (BrC), a type of OC, can absorb ultraviolet–visible radiation (Chen and Bond, 2010; Chen et al., 2020a). However, assessing the radiative effects of absorbing aerosols is challenging because of factors including a lack of high-resolution online data, lack of understanding of the optical properties of aerosols (Andreae and Gelencsér, 2006), uncertainty about aerosol emission sources (Li et al., 2016a), and poor parameterization in model simulations.

Lanzhou is the capital and largest city of Gansu Province in Northwest China, with a population of approximately 4.4 million. It is also a center for heavy industry and petrochemical production (Tan et al., 2016). Lanzhou was previously ranked as the most polluted city among the provincial capitals in China due to industrial pollution and its location in a narrow river valley, which forms a stable atmosphere with weak wind and a strong inversion layer, thus hindering the dispersion of air pollutants (Zhang et al., 2014). Several studies have been conducted on CA levels near the surface in Lanzhou (Pathak et al., 2011; Qiu et al., 2016; Tan et al., 2017). The optical properties and radiative effects of aerosols have also been evaluated (Gong et al., 2017; Pu et al., 2015). However, these studies have mainly used data obtained through offline sampling and laboratory measurements. In addition, the published data are inconsistent, because only several months in each study were selected to represent winter or summer, which caused large uncertainties in source attribution and model prediction results (Laskin et al., 2015; Yan et al., 2018). Studies have also reported the optical and radiative properties of particles but not the absorption properties of BrC. Therefore, the real-time observation of OC (including BrC) and BC is crucial not only for identifying their variations and source attribution but also for understanding the contribution of CAs to climate effects.

In this study, continual high-temporal-resolution measurements of OC and BC were conducted for the first time in Lanzhou from July 2018 to July 2019. The main objectives of this study were to (1) investigate ambient OC and BC concentrations in the atmosphere in Lanzhou and compare the data with those obtained in other regions; (2) assess the seasonal and diurnal variations of OC and BC and identify their potential sources; (3) calculate the absorption coefficients (b_{abs}), absorption Ångström exponent (AAE), and mass absorption cross-section of BrC (MAC_{BrC}); and (4) estimate the contributions of BrC and BC to the total light absorption of CAs.

1. Material and methods

1.1. Sampling site and meteorological condition

OC and BC measurements were conducted on the rooftop of the research building of the Northwest Institute of Eco-Environment and Resources, Chinese Academy of Sciences, Lanzhou (36.05°N, 103.858°E; 1540-m altitude above sea level) from July 15, 2018, to July 5, 2019. The site with sampling height of approximately 20 m can represent the air condition of Lanzhou City. The measurement site is maintained by the coordinated monitoring and research network for atmospheric pollution and cryospheric change over the Third Pole region (Kang et al., 2019). Instrument operators checked the instruments and created a monitoring log file each week. The instruments were maintained and calibrated at a time interval of two weeks. All data used in this study were recorded in Beijing Time (China Standard Time, UTC +8).

An automatic meteorological station was set on the rooftop of same building to obtain 10-min temperature, relative humidity, wind speed and direction. The accuracy of temperature sensor (Vaisala, Campbell Scientific Model HMP45C) was ± 0.4°C for temperature between −40°C and 60°C. The relative humidity sensor has uncertainties of ± 2% for relative humidity values from 0% to 90% and ± 3% from 90% to 100%. The annual rainfall was approximately 350 mm and mean temperature was 10.3°C during the sampling period (**Fig. S1**).

1.2. Total carbon–BC method for online high-temporal-resolution measurements

This study applied the total carbon (TC)–BC method, which combines a thermal method for TC detection using a new instrument, namely the Total Carbon Analyzer TCA08 (Aerosol d.o.o, Ljubljana, Slovenia; Rigler et al., 2020), with an optical method for measuring mass-equivalent BC using an AE33 aethalometer (Drinovec et al., 2015; Hansen et al., 1984).

The TCA08 instrument contains two parallel flow channels with two analytical chambers that alternate between sample collection and thermal analysis. While one channel is collecting its sample for the next time-base period, the other channel is analyzing the sample collected during the previous period. This sequential feature offers the advantage of continuous TC measurement. The instrument collects a sample of atmospheric aerosols on the 4.9-cm^2 central spot of a 47-mm-diameter quartz fiber filter enclosed in a small stainless-steel chamber; the sample collection process is executed at a controlled sampling flow rate of 16.7 L/min provided by a closed-loop stabilized internal pump. The sampling time was set on a 1-hr time base. At the end of the collection period, the sample flow is switched from one channel to the other. Each week, we changed new filters to ensure measurement quality. Detailed information was provided by Rigler et al. (2020)

The AE33 aethalometer measures BC aerosols in particulate matter with a diameter of ≤2.5 μm ($PM_{2.5}$) at a 1-min time base and at a sampling rate of 5 L/min. The aethalometer provides continuous estimates of BC mass at seven fixed wave-

lengths (370, 470, 520, 590, 660, 880, and 950 nm) in real time. In this instrument, BC mass is obtained by monitoring the attenuation of a beam of light transmitted through the aerosols collected on a quartz fiber filter at 880 nm.

In addition, Aethalometer provided wavelength dependent absorption coefficients which could be used to calculate biomass burning contribution($f_{biomass}$) to BC. The model assumes that the aerosol absorption coefficient can be viewed as the sum of fossil fuel and biomass combustion fractions. The total absorption at a wavelength can be represented as follows,

$$b_{abs(\lambda)} = b_{abs(\lambda,BB)} + b_{abs(\lambda,FF)} \quad (1)$$

where, $b_{abs\ (\lambda,\ BB)}$ and $b_{abs\ (\lambda,\ FF)}$ represent the BB and FF fraction of $b_{abs\ (\lambda)}$, respectively. b_{abs} values at 470 and 950 nm were used in source apportionment to estimate the percentage contribution of BB to BC as follows (Kumar et al., 2020; Pani et al., 2020).

$$\frac{b_{abs(470\ nm,\ BB)}}{b_{abs(950nm,\ BB)}} = \left(\frac{470}{950}\right)^{-AAE_{BB}} \quad (2)$$

$$\frac{b_{abs(470\ nm,\ FF)}}{b_{abs(950nm,\ FF)}} = \left(\frac{470}{950}\right)^{-AAE_{FF}} \quad (3)$$

$$BB(\%) = \frac{b_{abs(950nm,\ BB)}}{b_{abs(950nm)}} \times 100 \quad (4)$$

Biomass burning and fossil fuel EBC fractions are then calculated as:

$$BC_{BB} = BB\% \times BC \quad (5)$$

$$BCFF = (1 - BB)\% \times BC \quad (6)$$

This aethalometer has shown good agreement with other analytic techniques (Allen et al., 1999; Jeong et al., 2004) and has been extensively used worldwide (e.g., Babu et al., 2011; Nair et al., 2013). The principle of the aethalometer is described in detail by Hansen et al. (1984). In the present study, both the TCA08 and AE33 instruments collected samples through an inlet covered with a $PM_{2.5}$ cyclone on particle sizes.

1.3. *Estimation of spectral absorption*

The output BC concentration ($BC_{output,\ \lambda}$) was determined by dividing the total light absorption by the fixed values of the mass cross section of BC ($MAC_{BC,\ \lambda}$) provided by the manufacturer (Drinovec et al., 2015), signifying that the absorption coefficients (b_{abs}) could be calculated using Eq. (7):

$$b_{abs,\lambda} = BC_{output,\lambda} \times MAC_{BC,\lambda} \quad (7)$$

where, $b_{abs,\lambda}$ is the absorption coefficient at wavelength λ.

The fixed values of $MAC_{BC,\ \lambda}$ used in the AE-33 aethalometer were 18.47, 14.54, 13.14, 11.58, 10.35, 7.77, and 7.19 m^2/g for the wavelengths (λ) of 370, 470, 520, 590, 660, 880, and 950 nm, respectively. The wavelength dependence of b_{abs} is usually approximated by a power-law expression, which can be defined as follows:

$$b_{abs} = K \times \lambda^{-AAE} \quad (8)$$

where, K is a constant. The AAE for BC (AAE_{BC}) has mostly been set to 1, as recommended by previous studies (Li et al., 2018; Wang et al., 2018). At 880 nm, BC can be considered to be the only absorber, as suggested by previous studies (Liakakou et al., 2020; Xie et al., 2019). Therefore, the light absorption coefficients of BC ($b_{abs,BC,\lambda}$) under different pairs of wavelengths can be calculated using Eq. (9):

$$b_{abs},\ BC,\ \lambda 1 = b_{abs},\ BC,\ 880 \times \left(\frac{880}{\lambda_1}\right)^{AAE_{BC}} \quad (9)$$

The absorption coefficients of BrC ($b_{abs,BrC,\ \lambda}$) under different wavelengths can be calculated using Eq. (10):

$$b_{abs,BrC,\lambda} = b_{abs,\lambda} - b_{abs,BC,\lambda} \quad (10)$$

The contributions of BrC (BrC_{perc}) and BC (BC_{perc}) to the total light absorption of CAs can be estimated through Eqs. (11) and (12):

$$BrC_{perc} = \frac{b_{abs,\ Brc,\ \lambda}}{b_{abs,\ \lambda}} \quad (11)$$

$$BC_{perc} = 1 - BrC_{perc} = \frac{b_{abs,\ Bc,\ \lambda}}{b_{abs,\ \lambda}} \quad (12)$$

As demonstrated in previous studies, at wavelengths of 370–660 nm, BC and BrC are responsible for the total light absorption of CAs (Qiu et al., 2019; Wang et al., 2018). The wavelength dependence of BrC can be derived according to the AAE values of BrC (AAE_{BrC}; Andreae and Gelencsér, 2006; Lack and Cappa, 2010), which are estimated through Eq. (13):

$$AAE_{BrC,\ \lambda 1-\lambda 2} = \frac{\ln(b_{abs,BrC,\ \lambda 1}) - \ln(b_{abs,BrC,\ \lambda 2})}{\ln(\lambda 1) - \ln(\lambda 2)} \quad (13)$$

The values of the mass absorption cross-section of BrC (MAC_{BrC}) were estimated by dividing the absorption coefficients of BrC by the concentrations of OC (Eq. (14)), which were obtained using the TCA08 analyzer. Previous studies have used water-soluble OC (WSOC) to calculate BrC's mass absorption corss-section (MAC_{BrC}) because BrC is main component of WSOC (Cheng et al., 2017; Wu et al., 2019; Yan et al., 2018). WSOC constituted approximately 30%-70% of OC (Chen et al., 2020a, 2020b; Li et al., 2016b; Chen and Bond, 2010; Park et al., 2018); thus, the study estimated WSOC concentrations as a percentage (average 50%) of OC concentrations. Considering the estimation approach used by the aforementioned study, the values of MAC_{BrC} determined in the present study might have large uncertainties.

$$MAC_{BrC} = \frac{b_{abs,\ Brc,\lambda 1}}{WSOC} \quad (14)$$

2. Results and discussion

2.1. *Carbonaceous components*

The daily concentrations of OC and BC ranged from 1.44 to 25.91 and 0.31 to 12.64 μg/m^3, with an annual mean of

Table 1 – Black carbon (BC) concentration (μg/m^3) measured in Lanzhou compared with data from other studies in different places.

Sites	Type	Instrument	Time	Concentration	References
Lanzhou, China	Urban/$PM_{2.5}$	AE33	Jul 2018-Jul 2019	2.02 ± 1.26	This study
Nanjing, China	Urban/$PM_{2.5}$	AE33	2018	2.93 ± 0.60	Tan et al., 2020
Beijing, China	Urban/$PM_{2.5}$	AE31	2016	3.5	Xia et al., 2020
Wuhan, China	Urban/$PM_{2.5}$	AE31	2018	1.35→ ± 0.85	Zheng et al., 2020
Shanghai, China	Urban/TSP	AE33	2017	2.19 ± 1.28	Wei et al., 2020
Guangzhou, China	Urban/$PM_{2.5}$	AE31	2007-2008	4.7	Chen et al., 2014
Xuzhou, China	Urban/TSP	AE42	Apr 2014-Aug 2016	2.309	Chen et al., 2020c
Chengdu, China	Urban/TSP	AE31	2017	7.21	Guo et al., 2020
Xi'an, China	Urban/TSP	AE31	2016	10.47	Guo et al., 2020
Dunhuang, China	Rural/TSP	AE31	2017	4.43	Guo et al., 2020
Hami, China	Rural/TSP	AE31	2017	2.69	Guo et al., 2020
Ranwe, China	Remote/ TSP	AE31	Nov 2012-Jun 2013	0.139	Wang et al., 2016a
Beiluhe, China	Remote/ TSP	AE31	Nov 2012-Jun 2013	0.413	Wang et al., 2016a
QOMS, China	Remote/$PM_{2.5}$	AE33	Aug 2015-Jul 2017	0.298 ± 0.341	Chen et al., 2018
Waliguan, China	Remote/TSP	AE31	2017	0.31	Guo et al., 2020
Tianshan, China	Remote/$PM_{2.5}$	AE31	Aug 2016-Jul 2017	0.52	Zhang et al., 2020a
Akdala, China	Remote /TSP	AE31	2017	0.45	Guo et al., 2020
New Delhi, India	Urban/$PM_{2.5}$	AE33	Jan 2016-Dec 2018	13.58 ± 8.40	Kumar et al., 2020
Dehradun, India	Urban/$PM_{2.5}$	AE33	Oct 2017-Sep 2018	5.98 ± 3.17	Prabhu et al., 2020
Tehran, Iran	Urban/$PM_{2.5}$	AE31	Mar 2017-Mar2018	4.5 ± 1.7	Taheri et al., 2019
Athens, Greece	Urban/$PM_{2.5}$	AE33	May 2015-Apr 2019	1.9 ± 2.5	Liakakou et al., 2020
Agri, Italy	Rural/$PM_{2.5}$	AE33	Oct 2017-Oct 2018	0.867 ± 0.411	Pavese et al., 2020
Ranichauri, India	Rural/TSP	AE33	2016	1.93 ± 1.52	Pandey et al., 2020
Chirbasa, India	Remote/TSP	AE33	2016	0.395 ± 0.408	Negi et al., 2019

Abbreviations: TSP, total suspended particles.

(6.4 ± 4.4) and (2.0 ± 1.3) μg/m^3, respectively. Because our study is the first to apply an online OC measurement instrument for data collection in the study area, we could only compare our derived data with BC data from other sites (Table 1). The annual mean BC concentration in Lanzhou was lower than those in several other severely polluted urban areas in North China Plain and Yangtze River Delta Region in China such as Beijing, Xi'an, and Guangzhou. In addition, the BC concentration was much lower than that in New Delhi, and Dehradum in South Asia, and similar to those recorded in most other urban or rural areas. However, the concentration was significantly higher than those recorded in remote regions of the Tibetan Plateau (Table 1).

Several studies have reported OC and EC concentrations in $PM_{2.5}$ or in total suspended particles in Lanzhou on the basis of offline measurements. For instance, Zhang et al. (2020b) reported that the annual mean OC and EC concentrations in Lanzhou during 2019 were (8.6 ± 5.09) and (2.55 ± 1.44) μg/m^3, respectively, which are comparable to the data obtained in the current study. However, Tan et al. (2016) observed OC and EC concentrations as high as (35.4 ± 13.9) and (13.8 ± 5.41) μg/m^3 in December 2012 and (9.74 ± 3.30) and (4.44 ± 2.00) μg/m^3 in June 2013 in Lanzhou. Furthermore, another study reported high concentrations (OC: (17.7 ± 12.0) μg/m^3; BC: (9.0 ± 5.1) μg/m^3) in Chengguan District, Lanzhou, in 2014 (Wang et al., 2016b). Relatively high PM_1 OC and EC concentrations were also reported from December 2017 to January 2018 in Lanzhou (Zhao et al., 2019). The reasons for these disparities of the OC and EC concentrations in the different districts and periods are as follows: First, the aforementioned studies have been conducted in different years. Lanzhou's air quality has improved in recent years because of the relatively effective management of industrial and traffic emissions. Second, local emissions play a crucial role in some areas of the city. Third, offline measurements have higher levels of uncertainty than does online monitoring because the sampling process in offline measurements is usually conducted only once a week rather than continuously.

The OC-to-BC (OC/BC) ratio can provide information about pollution sources and strength (Chen et al., 2019; Turpin and Lim, 2001). In general, biomass burning has a higher OC/BC ratio than fossil fuel combustion; therefore, urban areas often have lower OC/BC ratios (range 1–4) than do rural or remote regions (Kunwar and Kawamura, 2014). In this study, the OC/BC ratios varied from 1.4 to 9.1, with the average ratio being 3.3 ± 1.2. The annual mean OC/BC ratio was similar to those derived in several urban areas in Asia, such as Beijing, Xi'an, Nanjing, Kathmandu, Karachi, and New Delhi, which are significantly affected by emissions from fossil fuel combustion (Cao et al., 2007; Chen et al., 2019; Chen et al., 2020a, 2020b; Sharma et al., 2014).

2.2. *Seasonal variations of OC and BC*

The OC and BC concentrations demonstrated clear seasonal variations over the sampling period (Fig. 1). For OC, the lowest concentrations occurred in May, remained relatively low during summer, and gradually increased through autumn to peak levels in December; in the following spring, the concentrations decreased again to a minimum in May and June. The seasonal variation of BC differed slightly, with the highest concentrations occurring in November 2018 and relatively low concen-

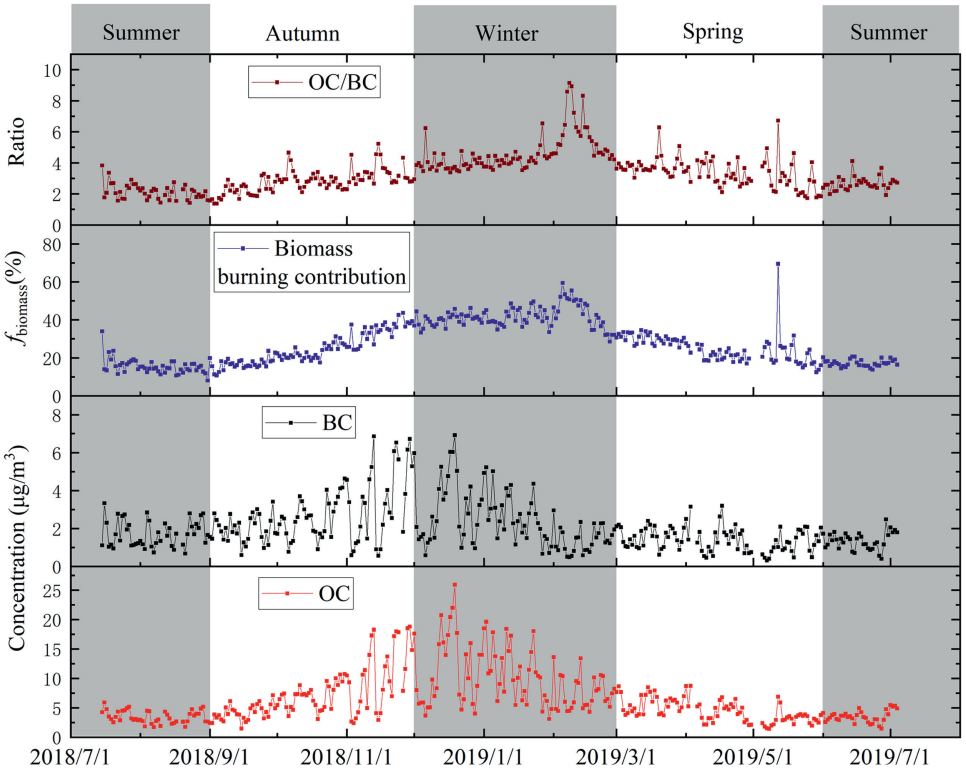

Fig. 1 – Seasonal variations of daily concentrations of organic carbon (OC), black carbon (BC), biomass burning contribution ($f_{biomass}$), and the OC/BC ratios during the sampling period in Lanzhou, China.

trations occurring in February 2019, leading to a high OC/BC ratio at that time. For both OC and BC, the highest monthly averages were approximately three times those of the lowest monthly averages. In addition, considerable fluctuations were observed from November 2018 to February 2019, suggesting that the emission, transmission, and diffusion rates were unstable and vary between seasons.

Similar seasonal variations for CAs such as OC, elemental carbon (EC), and humic-like substances have been reported in Lanzhou (Tan et al., 2016; Wang et al., 2016b; Zhang and Kang, 2018). The seasonal variations of pollutants have been demonstrated to result from variations in primary source emissions, in weather conditions, and in secondary formation processes. In this study, the relatively high OC and BC concentrations during autumn and winter reflect the combined effects of high local emissions and poor diffusion conditions. Coal was burned for heating due to a government policy that stipulates turning on coal-powered central heating in buildings from November 1 to March 31. In addition, the shallow boundary-layer height, relatively weak winds, and reduced precipitation during colder months as well as the region's valley topography created an environment conducive to the accumulation of air pollutants (**Fig. S1**; Chu et al., 2008; Zhao et al., 2019). Autumn and winter have relatively lower wind speed compared to other two seasons. Higher OC and BC concentrations were observed when wind speed ranged from 0.5 to 2 m/sec, while as the wind speed increase, their concentrations decreased (**Fig. S2**). By contrast, temperature inversion was reduced in summer, and convective activity was high, which was favorable for particle diffusion in the valley. Furthermore, local emissions decreased due to the absence of seasonal sources, such as coal combustion. In sum, we attributed the decrease in OC and BC concentrations in summer to the reduced temperature inversion, strong convective activity, and decreased emission strength as suggested by (Zhao et al., 2019).

In addition, the derived OC/BC ratios exhibited a clear seasonal variation in Lanzhou (Fig. 1). The ratios were lowest in summer, increased through autumn, and reached a peak around late winter (February). The relatively low ratio in summer suggests that fossil fuel combustion, such as vehicle emissions, mainly contributed to the atmospheric OC and BC in this period. In winter, although large amounts of coal were burned for heating, biomass burning may have contributed considerably to atmospheric OC and BC, resulting in the high OC/BC ratio (Chen et al., 2015). To further prove this, we also calculated the secondary OC (SOC) contribution using OC/BC_{min} method because BC is largely from primary emission, while OC has both primary and secondary sources thus affected more by chemical processes. The seasonal mean SOC concentrations were (2.1 ± 1.2), (1.3 ± 0.6), (3.6 ± 2.5), and (3.0 ± 1.3) μg/m^3 in spring, summer, autumn, and winter, respectively. Winter had the lowest SOC contribution to OC with value of 33.1%, followed by summer, spring, and autumn (**Table 2**). The daily contribution from biomass burning ($f_{biomass}$) ranged from 8.1% to 69.5% (mean value: 27.1% ± 11.3%; **Fig. 1**), further confirming that atmospheric BC in Lanzhou was mainly derived from fossil fuel combustion. Moreover, $f_{biomass}$ exhibited the same seasonal variation as the OC/BC ratio, with winter having the highest value

Table 2 – Summary of carbonaceous aerosols (CAs) and light absorption parameters measured in Lanzhou, China.

	Annual	Spring	Summer	autumn	Winter
OC ($\mu g/m^3$)	6.41 ± 4.35	4.54 ± 1.90	3.50 ± 1.02	7.13 ± 4.27	10.0 ± 5.09
BC ($\mu g/m^3$)	2.02 ± 1.26	1.42 ± 0.63	1.56 ± 0.62	2.62 ± 1.47	2.40 ± 1.49
SOC ($\mu g/m^3$)	2.54 ± 1.78	2.12 ± 1.20	1.29 ± 0.59	3.56 ± 2.45	3.01 ± 1.31
OC/BC	3.32 ± 1.23	3.38 ± 0.91	2.37 ± 0.54	2.80 ± 0.74	4.61 ± 1.22
SOC/OC	0.41 ± 0.15	0.46 ± 0.15	0.38 ± 0.14	0.48 ± 0.14	0.33 ± 0.13
$f_{biomass}$ (%)	27.1 ± 11.3	25.1 ± 7.47	16.2 ± 3.41	24.4 ± 8.11	41.6 ± 5.71
$b_{abs,\ BC,\ 370}$ (Mm^{-1})	38.0 ± 23.4	27.3 ± 12.1	30.4 ± 12.6	48.1 ± 27.7	45.1 ± 27.6
$b_{abs,\ BrC,\ 370}$ (Mm^{-1})	19.6 ± 19.1	12.1 ± 6.84	7.08 ± 2.81	21.9 ± 20.4	35.6 ± 22.0
f_{BrC} (%)	30.8 ± 11.1	30.2 ± 7.42	19.2 ± 4.18	28.1 ± 8.79	44.2 ± 4.08
$AAE_{(370\text{-}520)}$	4.19 ± 0.46	4.38 ± 0.43	3.91 ± 0.44	4.09 ± 0.54	4.34 ± 0.20
$MAC_{BrC,\ 370}$ (m^2/g)	5.37 ± 1.91	5.14 ± 1.63	3.90 ± 0.70	5.32 ± 1.80	6.76 ± 1.62

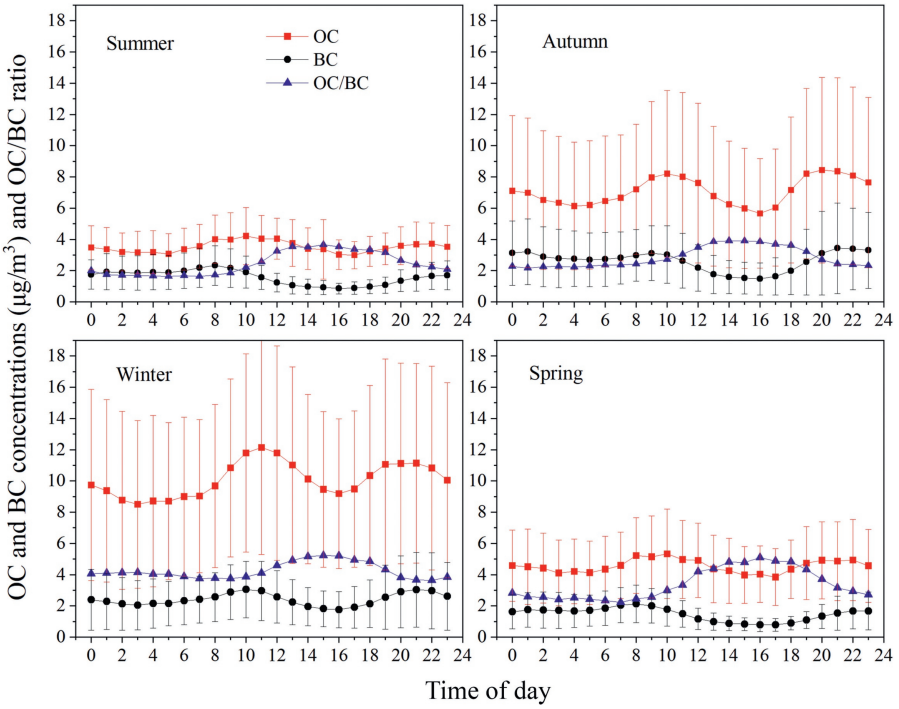

Fig. 2 – Diurnal profiles of mean hourly organic carbon (OC), black carbon (BC), and OC/BC ratio in Lanzhou, China, by season during the measurement period.

(41.6% ± 5.7%), followed by spring (25.1% ± 7.5%), autumn (24.4% ± 8.1%), and summer (16.2% ± 3.4%). This reflects the change in emission sources between different seasons and demonstrates that biomass burning played a crucial role in OC and BC concentrations, particularly in winter.

2.3. *Diurnal variations of OC, BC, and OC/BC ratios*

Diurnal variations are keys to understanding the influences of human activities and surface meteorological processes on OC and BC concentrations in Lanzhou. The patterns of the diurnal variations of OC and BC in all seasons were similar: one daily peak occurred in the morning hours and another at night (**Fig. 2**). Previous studies have reported similar types of diurnal OC and BC variations with two peaks but with a slight shift in time and magnitude in different locations in Asia (Chen et al., 2020c; Prabhu et al., 2020; Sun et al., 2020; Taheri et al., 2019; Wei et al., 2020; Xiao et al., 2020; Zhang et al., 2020a). However, variation patterns observed at high-altitude stations such as Beiluhe and Ranwu (Wang et al., 2016a), and Lulang (Zhao et al., 2017) exhibited only one peak in the early morning hours.

The morning peak is attributable to the morning rush hour, fuel burning for making breakfast, and particles from the residual nocturnal layer being lifted by enhanced convective activity as the air warms (Beegum et al., 2009). After the morning peak, the OC and BC concentrations began to decrease and reached a minimum at approximately 16:00; this is attributable to decreased traffic emissions and increased boundary-layer height (Kumar et al., 2020; Williams et al., 2019). In the evening, the OC and BC concentrations again increased because of the evening rush hour and the atmospheric boundary layer becoming thinner due to a decrease in vertical convection as the air cooled. The evening peak remained until late in the night as anthropogenic activities decreased (Rehman et al., 2011). The first peak in winter was delayed by approximately 1 hr for both OC and BC, mainly be-

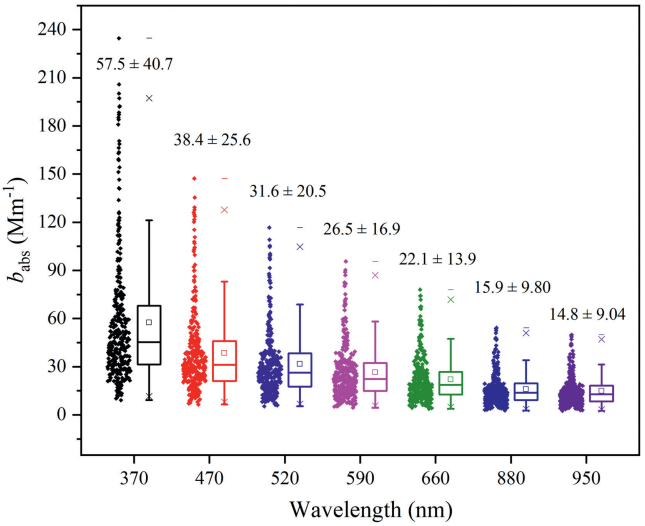

Fig. 3 – Box-and-whisker plot of absorption coefficients at seven wavelengths as measured with an AE33 aethalometer.

cause the sunrise and sunset times vary with the seasons. Furthermore, the magnitude of the peaks decreased in accordance with the overall inter-seasonal decrease in CA from winter to summer.

OC and BC did not exhibit the same diurnal variations. The OC peaks occurred at approximately 10:00 and 20:00 (**Fig. 2**). By contrast, the first BC peak was 1 or 2 hr earlier, and the second peak was delayed by approximately 1 hr, suggesting that OC and BC have different sources. Traffic emissions contributed considerably to both OC and BC in the morning and evening. However, a considerable proportion of OC was contributed by secondary formation as temperatures rose during the day, thus caused the first peak delay of OC. Correspondingly, the SOC decrease after sunset therefore leading to the ahead of second peak in comparation to BC. By contrast, BC concentrations were always higher at night, which can be attributed to increased emissions from domestic cooking and heating and accumulation resulting from the lower nocturnal atmospheric boundary-layer height.

The patterns of the diurnal variations of OC/BC in all seasons were similar with stable values in hours from 22:00 to 8:00 or 9:00 of next day, increasing gradually and reaching peak around 15:00 or 16:00, then start decreasing again (**Fig. 2**). Both OC and BC concentrations decreased in the afternoon, however, BC decreased more compared to OC, thus causing a higher OC/BC ratio. This might reflect the contribution of SOC to OC particularly in the afternoon.

2.4. *Light absorption characteristics*

2.4.1. *Spectral dependence of light absorption*

A box-and-whisker plot of aerosol absorption coefficients (b_{abs}) at wavelengths ranging from 370 to 950 nm is presented in **Fig. 3**. The b_{abs} values were highest at shorter wavelengths (370 nm) and decreased as the wavelengths increased. The annual mean absorption coefficient was (57.5 ± 40.7) Mm^{-1} (10^{-6} m^{-1}) at 370 nm, (38.4 ± 25.6) Mm^{-1} at 470 nm, (31.6 ± 20.5) Mm^{-1} at 520 nm, (26.5 ± 16.9) Mm^{-1} at 590 nm, (22.1 ± 13.9) Mm^{-1} at 660 nm, (15.9 ± 9.8) Mm^{-1} at 880 nm, and (14.8 ± 9.0) Mm^{-1} at 950 nm. In certain cases, the b_{abs} values were extremely high (>150 Mm^{-1}) at shorter wavelengths, implying that the atmosphere was heavily laden with CAs. The same pattern has been reported by several other studies, although the b_{abs} values differ from those observed in the present study (Dumka et a., 2018; Liakakou et al., 2020; Qin et al., 2018; Zhang et al., 2021). For instance, compared with the values observed in the present study, Titos et al. (2014) reported considerably lower seasonal mean $b_{abs,\,637}$ values of 17 and 11 Mm^{-1} for winter and spring, respectively, in Granada, Spain. Moreover, Segura et al. (2016) reported a lower $b_{abs,\,520}$ value (18.6 ± 0.3 Mm^{-1}) in Valencia, Spain, which is approximately half of the value in the current study. By contrast, comparable values to those observed in our study have been recorded in Athens, Greece (Katsanos et al., 2019; Liakakou et al., 2020) and Guangzhou, China (Qin et al., 2018). Extremely high values were also observed in urban areas of South Asia; in Delhi, mean $b_{abs,520}$ and $b_{abs,880}$ values of (355 ± 179) and (190 ± 95) Mm^{-1}, respectively, were reported (Dumka et al., 2018). The differences between the reported b_{abs} values reflect variations in aerosol concentrations or absorbing characteristics in different regions.

2.4.2. *Seasonal variation of* $b_{abs,\,370}$ *and the light absorption contribution of BrC*

Fig. 4a presents the daily series of $b_{abs,\,370}$ values observed for BC and BrC, which ranged from 2.12 to 129 and 0.72 to 106 Mm^{-1}, respectively, with annual means of (38.0 ± 23.4) and (19.6 ± 19.1) Mm^{-1}, respectively. Both b_{abs} values were low in summer, increased through autumn, reached a maximum in December, and gradually decreased to a second minimum in July. Liakakou et al. (2020) proposed that a lower mixing-layer height in winter might affect b_{abs} by increasing the concentrations of absorbing materials. In addition, changes in aerosol sources, such as from biomass burning, might play a role in the variation of b_{abs} values (Lack et al., 2012). This was confirmed by the derived $f_{biomass}$ values, which revealed that the percentage of aerosols originating from biomass burning increased from 16.2% ± 3.4% in summer to 41.6% ± 5.7% in winter.

The contribution of BrC to CA light absorption exhibited a similar seasonal variation, with winter having the highest contribution (44.2% ± 4.1%), followed by spring (30.2% ± 7.4%), autumn (28.1% ± 8.8%), and summer (19.2% ± 4.2%; **Fig. 4b and Table 2**). This variation was attributed to the influence of enhanced biomass burning in winter and increased fossil fuel combustion and increased secondary organic aerosol (SOA) formation in summer. Tan et al. (2017) reported the SOA contribution to the total light absorption of organic aerosols to be 31% in summer and 23% in winter. Our measurements revealed a higher BrC contribution than those measured in many other urban areas. For instance, Qin et al. (2018) estimated that BrC contributed 23.6% of the light absorption at 370 nm in Guangzhou, China. Liakakou et al. (2020) reported that BrC contributed 33.5% in winter and 18.5% in summer at 370 nm in urban Athens, Greece. Shamjad et al. (2016) revealed that BrC contributed 30% of the total light absorption at 365 nm in Kanpur, India. Several other studies on the contribution of BrC to total light absorption at 405 nm have re-

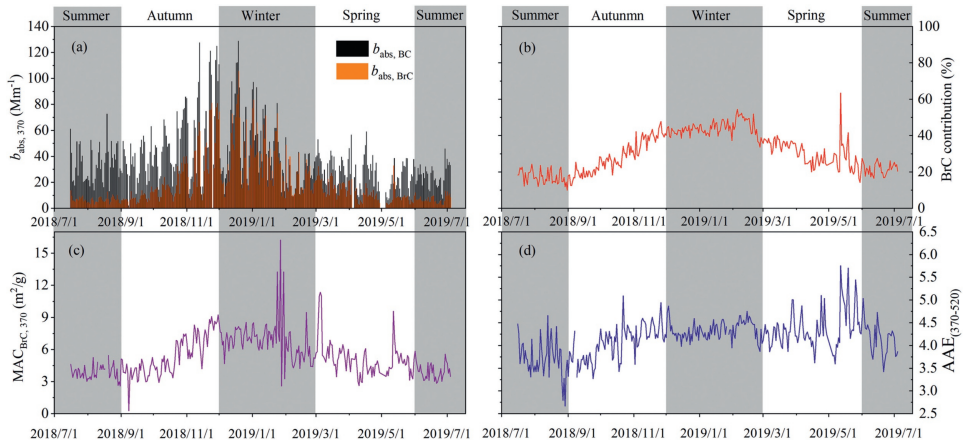

Fig. 4 – Seasonal variations of (a) the absorption coefficients (b_{abs}) of black carbon (BC) and brown carbon (BrC; Mm^{-1}), (b) the BrC absorption contribution (%), (c) the mass cross section of BrC ($MAC_{BrC,370}$; m^2/g), and (d) absorption Ångström exponent (AAE: 370–520 nm).

ported values ranging from approximately 10% in California, the United States (Cappa et al., 2012) to 27% ± 15% in Boulder, the United States (Lack et al., 2012) and up to approximately 50% in Jeju, South Korea (Flowers et al., 2010). Moreover, numerous studies have estimated a BrC contribution of approximately 10% to 30% at near-UV and approximately 10% at 550-nm wavelengths (Yang et al., 2009; Bahadur et al., 2012; Lack et al., 2012; Li et al., 2018; Washenfelder et al., 2015; Cheng et al., 2011; Du et al., 2014). In general, rural and remote areas exhibited higher BrC contributions due to the greater impact of biomass burning from agricultural activities (Yuan et al., 2016). In the present study, the large contributions of BrC to light absorption estimated in Lanzhou demonstrate that biomass burning in winter produced highly absorbent BrC aerosols.

2.4.3. *Characteristics of other optical parameters*

MAC values for BrC were calculated using $b_{abs,BrC,370}$ and estimated WSOC. Clear seasonal variations of MAC_{BrC} were observed in Lanzhou (**Fig. 4c**), possibly due to the effect of photobleaching on BrC and interseasonal source variations. The estimated MAC_{BrC} values at 370 nm in Lanzhou were higher in winter than in other seasons (**Table 2**), with the annual mean value being 5.4 ± 1.9 m^2/g. Photochemical oxidation, the washing-out effect of BrC, and varying SOC contributions affect the seasonal variation of MAC_{BrC} (Saleh et al., 2015). Relatively intense sunlight, high humidity levels, and elevated temperatures cause intensive photochemical oxidation and SOC formation, thus reducing MAC_{BrC} in summer (Forrister et al., 2015). Correspondingly, in winter, a higher percentage of BrC is derived from biomass burning than from vehicle emissions or atmospheric reactions, and BrC derived from biomass burning is more absorbent (Cheng et al., 2011; Hecobian et al., 2010; Hu et al., 2017). In Lanzhou, increased biomass burning in winter resulted in the higher MAC_{BrC} values. The seasonal variation of MAC_{BrC} is consistent with measurements conducted at other sites (e.g., Bikkina et and Sarin 2014; Cheng et al., 2011; Liakakou et al., 2020). However, the estimated MAC_{BrC} values varied between regions. For instance, MAC_{BrC} values similar to those observed in our study were reported in winter in Sanmenxia, China (4.33 m^2/g; Zhang et al., 2021) and Athens, Greece (4.25 m^2/g; Liakakou et al., 2020). However, several studies have reported lower MAC_{BrC} values for water-soluble OC (Cheng et al., 2011; Choudhary et al., 2017; Dasari et al., 2019; Kirillova et al., 2014; Moschos et al., 2018; Satish et al., 2017; Srinivas et al., 2016; Zhang et al., 2011).

To examine the influence of each CA component on the spectral dependence of $b_{abs,BrC}$, daily series of AAE_{BrC} values were measured at wavelengths ranging from 370 to 520 nm, as displayed in **Fig. 4d**. The measured AAE_{BrC} values ranged from 2.7 to 7.7, with the annual mean being 4.2 ± 0.5; it was highest in spring (4.4 ± 0.4) and decreased in summer (3.9 ± 0.4). This indicates a larger slope in $b_{abs,BrC}$ spectral variation and reveals the influence of emissions from biomass burning. Core-shell mixing of BrC with BC may enhance total light absorption (lensing effect) and reduce the spectral dependence of $b_{abs,BrC}$ (Cheng et al., 2011; Choudhary et al., 2017) during daylight hours throughout the year. In our study, the large seasonal changes in AAE_{BrC} indicate a large variability in chromophores in Lanzhou, which alter the spectral dependence of $b_{abs,BrC}$ (Liakakou et al., 2020). Photooxidation processes and boundary-layer dynamics may also play a key role in the AAE_{BrC} variations. The considerably higher AAE_{BrC} values at the end of May (mean of 5.8 ± 0.9) are attributable to the large percentage of more absorbent, processed organic aerosols from synoptic-scale northern advections.

Highly similar AAE_{BrC} values to those in the present study have been observed in Mediterranean urban environments. Massabó et al. (2015) reported a mean AAE_{BrC} value of 4.0 ± 0.2 in Genoa, Italy. Bernardoni et al. (2017) found an AAE_{BrC} of 3.8 ± 0.11 in Milan. Moreover, Costabile et al. (2017) reported an AAE_{BrC} value of 3.2 ± 0.9 in Bologna, Italy. However, compared with the values in the present study, higher AAE_{BrC} values have been estimated in polluted urban environments in Asia such as those in Delhi (5.1 ± 2.0; Kirillova et al., 2014), Kharagpur (6.0 ± 1.1; Bikkina and Sarin, 2014), and Beijing (7.0 ± 0.8; Cheng et al., 2011). Yan et al. (2018) provided a review of AAE_{BrC} values from several sources and concluded that the AAE value for BrC originating from fossil fuel combustion was approximately 1 and that for BrC originating from incomplete biomass burning ranged from 1 to 3 (Martinsson et al., 2015). The AAE value for secondary BrC ranged from 3 to 7. These

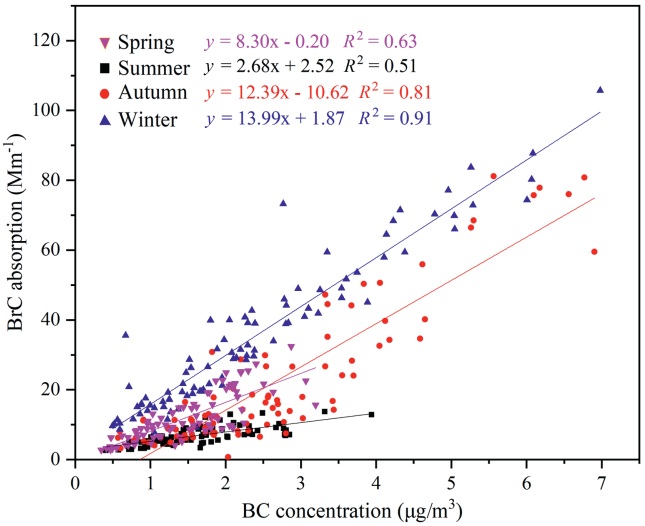

Fig. 5 – Correlation between BrC absorption at 370 nm and BC mass at 880 nm in each season.

slightly higher AAE values possibly reflect the combined influence of a large contribution of biomass burning and the oxidation of primary BrC into secondary BrC (Zhang et al., 2011).

2.5. *Changes in BrC spectral absorption*

The optical and physical properties of BrC and BC differ due to the formation and/or loss of secondary components through photobleaching and volatilization (Andreae and Gelencsér, 2006; Lee et al., 2014; Zhao et al., 2015). Accordingly, the relationship between BrC absorption and BC mass can be used to determine the extent to which combustion sources influence the spectral absorbance and variations of BrC. Results obtained from a regression analysis between $b_{abs,BrC,370}$ and BC mass for four seasons is illustrated in **Fig. 5**, revealing large differences in slopes and data scatter.

The absorption pattern of BrC was heteroscedastic, with BC increasing during winter; this is because the variability of $b_{abs,BrC}$ may reach approximately 100 Mm^{-1} within higher concentration ranges. This large variability can be attributed to the influence of different sources, different mixing states, and the chemical composition of the BrC species (Shamjad et al., 2016). BrC is susceptible to photochemical aging, leading to a decrease in its absorbance capacity; nevertheless, increased BrC emissions combined with core-shell mixing between BC and inorganic species may improve its absorption (Pokhrel et al., 2017). A stronger dependence was observed betweeen $b_{abs,BrC}$ and BC mass in winter ($R^2 = 0.91$) compared with other seasons. In summer, $b_{abs,BrC}$ seemed to be relatively independent of BC ($R^2 = 0.51$), implying different emission sources between the two components.

3. Conclusions

This study used a newly developed total carbon analyzer (TCA08) coupled with an aethalometer (AE33) to detect OC and BC concentrations in $PM_{2.5}$ in a valley city in northwest China from July 2018 to July 2019. The annual mean OC and BC concentrations during the measurement period were 6.4 ± 4.4 and 2.0 ± 1.3 μg/m³, respectively. Both components exhibited clear seasonal variations, with winter having maximum concentrations, followed by autumn, spring, and summer. In addition, the concentrations peaked twice daily in all four seasons, although the timing of the daily peaks differed slightly between OC and BC because of the different sources of each. A relatively low OC/BC ratio (3.3 ± 1.2) was also observed, suggesting that fossil fuel combustion contributed greatly to CAs in Lanzhou. The contribution from biomass burning increased substantially in winter, which was further supported by the measured $f_{biomass}$. The aerosol absorption coefficients exhibited a strong spectral dependence with widely varying b_{abs} values that occasionally exceeded 120 Mm^{-1} at 370 nm and registered a mean of (31.6 ± 20.5) Mm^{-1} at 520 nm. The light absorption properties of BrC were significantly enhanced in the near-ultraviolet and visible spectral regions; the annual mean contribution of BrC at 370 nm was 30.8% ± 11.1% and could reach 44.2% ± 4.1% in winter due to increased biomass burning. Higher $MAC_{BrC,\ 370}$ values and $AAE_{(370\text{-}520)}$ values were observed in winter than in summer, further reflecting increased biomass burning. In addition to combustion sources, different mixing states and the chemical composition of the BrC species play a major role in the light absorption of BrC aerosols. This study provides firstly valuable data on seasonal, diurnal variation, and optical characteristics of BC and BrC in a typical city in northwest China. These data are crucial for studies of climate change simulation, public health effect estimation and relatively emission reduction.

Acknowledgments

This study was supported by the Pan-Third Pole Environment Study for a Green Silk Road (Pan-TPE) (No. XDA20040501), the Frontier Science Key Project of CAS (No. QYZDJ-SSW-DQC039), the Gansu Science and Technology Plan (No. 18JR2RA005), the CAS "Light of West China" program, and the State Key Laboratory of Cryospheric Science (No. SKLCS-ZZ-2022). This study is part of a framework across the Tibetan Plateau: Atmospheric Pollution and Cryospheric Change (APCC). This manuscript was edited by Wallace Academic Editing.

Appendix A Supplementary data

Supplementary material associated with this article can be found, in the online version, at doi:10.1016/j.jes.2022.08.007.

REFERENCES

Allen, G.A., Lawrence, J., Koutrakis, P., 1999. Field validation of a semi-continuous method for aerosol black carbon (aethalometer) and temporal patterns of summertime hourly black carbon measurements in southwestern PA. Atmos. Environ. 33, 817–823.

Andreae, M.O., Gelencsér, A., 2006. Black carbon or brown carbon? The nature of light absorbing carbonaceous aerosols. Atmos. Chem. Phys. 6, 3131–3148.

Babu, S.S., Moorthy, K.K., Manchanda, R.K., Sinha, P.R., Satheesh, S.K., Vajja, D.P., et al., 2011. Free tropospheric black carbon aerosol measurements using high altitude balloon: Do BC layers build “their own homes” up in the atmosphere? Geophys. Res. Lett. 38, L08803.

Bahadur, R., Praveen, P.S., Xu, Y., Ramanathan, V., 2012. Solar absorption by elemental and brown carbon determined from spectral observations. Proc. Nat. Acad. Sci. 109, 17366–17371.

Beegum, S.N., Moorthy, K.K., Babu, S.S., Sathesh, S.K., Vinoj, V., Badarinath, K.V.S., et al., 2009. Spatial distribution of aerosol black carbon over India during pre-monsoon season. Atmos. Environ. 43, 1071–1078.

Bernardoni, V., Pileci, R.E., Caponi, L., Massabò, D., 2017. The Multi-Wavelength Absorption Analyzer (MWAA) model as a tool for source and component apportionment based on aerosol absorption properties: application to samples collected in different environments. Atmosphere 8, 218.

Bikkina, S., Sarin, M.M., 2014. Brown carbon in atmospheric outflow from the IndoGangetic Plain: mass absorption efficiency and temporal variability. Atmos. Environ. 89, 835–843.

Bond, T.C., Bergstrom, R.W., 2006. Light absorption by carbonaceous particles: An investigative review. Aerosol Sci. Technol. 40, 27–67.

Bond, T.C., Doherty, S.J., Fahey, D.W., Forster, P.M., Berntsen, T., DeAngelo, B.J., et al., 2013. Bounding the role of black carbon in the climate system: A scientific assessment. J. Geophy. Res. Atmos. 118, 5380–5552.

Cao, J.J., Lee, S.C., Chow, J.C., Watson, J.G., Ho, K.F., Zhang, R.J., et al., 2007. Spatial and seasonal distributions of carbonaceous aerosols over China. J. Geophy. Res. Atmos. 112, D22S11.

Cappa, C.D., Onasch, T.B., Massoli, P., Worsnop, D.R., Bates, T.S., Cross, E.S., et al., 2012. Radiative absorption enhancements due to the mixing state of atmospheric black carbon. Science 337, 1078–1081.

Chen, Y., Bond, T.C., 2010. Light absorption by organic carbon from wood combustion. Atmos. Chem. Phys. 10, 1773–1787.

Cheng, Y., He, K.B., Zheng, M., Duan, F.K., Du, Z.Y., Ma, Y.L., et al., 2011. Mass absorption efficiency of elemental carbon and watersoluble organic carbon in Beijing, China. Atmos. Chem. Phys. 11, 11497–11510.

Cheng, Y., He, K.B., Engling, G., Weber, R., Liu, J.M., Du., Z.Y., et al., 2017. Brown and black carbon in Beijing aerosol: Implications for the effects of brown coating on light absorption by black carbon. Sci. Total Environ. 599-600, 1047–1055.

Chen, P.F., Kang, S.C., Gul, C., Tripathee, L., Wang, X.X., Hu, Z.F., Li, C.L., Pu, T., 2020a. Seasonality of carbonaceous aerosol composition and light absorption properties in Karachi, Pakistan. J. Environ. Sci. 90, 286–296.

Chen, P.F., Kang, S.C., Tripathee, L., Ram, K., Rupakheti, M., Panday, A.K., et al., 2020b. Light absorption properties of elemental carbon (EC) and watersoluble brown carbon (WS-BrC) in the Kathmandu Valley, Nepal: A 5- year study. Environ. Pollut. 261, 114239.

Chen, P.F., Kang, S.C., Li, C.L., Zhang, Q.G., Guo, J.M., Tripathee, L., et al. , 2019. Carbonaceous aerosol characteristics on the Third Pole: A primary study based on the Atmospheric Pollution and Cryospheric Change (APCC) network. Environ. Pollut. 253, 49–60.

Chen, X.C., Zhang, Z.S., Engling, G., Zhang, R.J., Tao, J., Lin, M., et al., 2014. Characterization of fine particulate black carbon in Guangzhou, a megacity of South China. Atmos. Pollut. Res. 5, 361–370.

Chen, Y.J., Tian, C.G., Feng, Y.L., Zhi, G.R., Li, J., Zhang, G., 2015. Measurements of emission factors of PM2.5, OC, EC, and BC for household stoves of coal combustion in China. Atmos. Environ. 109, 190–196.

Chen, W., Tian, H.M., Zhao, H.M., Qin, K., 2020c. Multichannel characteristics of absorbing aerosols in Xuzhou and implication of black carbon. Sci. Total Environ. 714, 136820.

Chen, X., Kang, S., Cong, Z., Yang, J., Ma, Y., 2018. Concentration, temporal variation and sources of black carbon in the Mount Everest region retrieved by real-time observation and simulation. Atmos. Chem. Phys. 18, 12859–12875.

Choudhary, V., Rajput, P., Rajeev, P., Gupta, T., 2017. Synergistic effect in absorption properties of brown carbon and elemental carbon over IGP during weak southwest monsoon. Aerosol Sci. Eng. 1, 138–149.

Chu, P.C., Chen, Y., Lu, S., 2008. Atmospheric effects on winter SO2 pollution in Lanzhou, China. Atmos. Res. 89, 365–373.

Costabile, F., Gilardoni, S., Barnaba, F., Di Ianni, A., Di Liberto, L., Dionisi, D., et al., 2017. Characteristics of brown carbon in the urban Po Valley atmosphere. Atmos. Chem. Phys. 17, 313–326.

Dasari, S., Andersson, A., Bikkina, S., Holmstrand, H., Budhavant, K., Satheesh, S., et al., 2019. Photochemical degradation affects the light absorption of water-soluble brown carbon in the South Asian outflow. Sci. Adv. 5, eaau8066.

Drinovec, L., Mo?nik, G., Zotter, P., Prévôt, A.S.H., Ruckstuhl, C., Coz, E., et al., 2015. The "dual-spot" Aethalometer: an improved measurement of aerosol black carbon with real-time loading compensation. Atmos. Meas. Tech. 8, 1965–1979.

Du, Z., He, K., Cheng, Y., Duan, F., Ma, Y., Liu, J., et al., 2014. A yearlong study of water-soluble organic carbon in Beijing I: sources and its primary vs. secondary nature. Atmos. Environ. 92, 514–521.

Dumka, U.C., Kaskaoutis, D.G., Tiwari, S., Safai, P.D., Attri, S.D., Soni, V.K., et al., 2018. Assessment of biomass burning and fossil fuel contribution to black carbon concentrations in Delhi during winter. Atmos. Environ. 194, 93–109.

Flowers, B.A., Dubey, M.K., Mazzoleni, C., Stone, E.A., Schauer, J.J., Kim, S.W., et al., 2010. Optical-chemical-microphysical relationships and closure studies for mixed carbonaceous aerosols observed at Jeju Island; 3-laser photoacoustic spectrometer, particle sizing, and filter analysis. Atmos. Chem. Phys. 10, 10387–10398.

Forrister, H., Liu, J., Scheuer, E., Dibb, J., Ziemba, L., Thornhill, K.L., et al., 2015. Evolution of brown carbon in wildfire plumes. Geophys. Res. Lett. 42, 4623–4630.

Gong, C., Xin, J., Wang, S., Wang, Y., Zhang, T., 2017. Anthropogenic aerosol optical and radiative properties in the typical urban/suburban regions in China. Atmos. Res. 197, 177–187.

Guo, B., Wang, Y.Q., Zhang, X.Y., Che, H,Z., Ming, J., Yi, Z.W., 2020. Long-Term Variation of Black Carbon Aerosol in China Based on Revised Aethalometer Monitoring Data. Atmosphere. 11, 684.

Hansen, A.D.A., Rosen, H., Novakov, T., 1984. The aethalometer-An instrument for the real-time measurement of optical absorption by aerosol particles. Sci. Total Environ. 36, 191–196.

Hodnebrog, Ø., Myhre, G., Samset, B.H., 2014. How shorter black carbon lifetime alters its climate effect. Nat. Commun. 5, 5065.

Hecobian, A., Zhang, X., Zheng, M., Frank, N., Edgerton, E.S., Weber, R.J., 2010. Watersoluble organic aerosol material and the light-absorption characteristics of aqueous extracts measured over the Southeastern United States. Atmos. Chem. Phys. 10, 5965–5977.

Hu, Z.F., Kang, S.C., Li, C.L., Yan, F.P., Chen, P.F., Gao, S.P., et al., 2017. Light absorption of biomass burning and vehicle emission- € sourced carbonaceous aerosols of the Tibetan Plateau. Environ. Sci. Pollut. Res. 24, 15369–15378.

Jeong, C.-H., Hopke, P.K., Kim, E., Lee, D.-W., 2004. The comparison between thermal-optical transmittance elemental carbon and Aethalometer black carbon measured at multiple monitoring sites. Atmos. Environ. 38, 5193–5204.

Kang, S., Zhang, Q., Qian, Y., Ji, Z., Li, C., Cong, Z., et al., 2019. Linking atmospheric pollution to cryospheric change in the Third Pole region: current progress and future prospects. Natl. Sci. Rev. 6, 796–809.

Katsanos, D., Bougiatioti, A., Liakakou, E., Kaskaoutis, D.G., Stavroulas, I., Paraskevopoulou, D., et al., 2019. Optical properties of near-surface urban aerosols and their chemical tracing in a Mediterranean City (Athens). Aeros. Air Qual. Res. 19, 49–70.

Kirillova, E.N., Andersson, A., Tiwari, S., Srivastava, A.K., Bisht, D.S., Gustafsson, Ö., 2014. Water-soluble organic carbon aerosols during a full New Delhi winter: Isotope-based source apportionment and optical properties. J. Geophys. Res. 119, 3476–3485.

Kumar, R.R., Soni, V.K., Jain, M.K., 2020. Evaluation of spatial and temporal heterogeneity of black carbon aerosol mass concentration over India using three year measurements from IMD BC observation network. Sci. Total Environ. 723, 138060.

Kunwar, B., Kawamura, K., 2014. Seasonal distributionsand sources of low molecular weight dicarboxylic acids, ω-oxocarboxylic acids, pyruvicacid, α-dicarbonyls and fatty acids in ambient aerosols from subtropical Okinawa in the western Pacific Rim. Environ. Chem. 11 (6), 673–689.

Lack, D.A., Langridge, J.M., Bahreini, R., Cappa, C.D., Middlebrook, A.M., Schwarz, J.P., 2012. Brown carbon and internal mixing in biomass burning particles. Proc. Nat. Acad. Sci. 109, 14802–14807.

Lack, D.A., Cappa, C.D., 2010. Impact of brown and clear carbon on light absorption enhancement, single scatter albedo and absorption wavelength dependence of black carbon. Atmos. Chem. Phys. 10, 4207–4220.

Laskin, A., Laskin, J., Nizkorodov, S.A., 2015. Chemistry of atmospheric brown carbon. Chem. Rev. 115, 4335–4382.

Lee, H.J., Aiona, P.K., Laskin, A., Laskin, J., Nizkorodov, S.A., 2014. Effect of solar radiation on the optical properties and molecular composition of laboratory proxies of atmospheric brown carbon. Environ. Sci. Technol. 48, 10217–10226.

Lelieveld, J., Evans, J.S., Fnais, M., Giannadaki, D., Pozzer, A., 2015. The contribution of outdoor air pollution sources to premature mortality on a global scale. Nature 525, 367–371.

Liakakou, E., Stavroulas, I., Kaskaoutis, D.G., Grivas, G., Paraskevopoulou, D., Dumka, U.C., et al., 2020. Long-term variability, source apportionment and spectral properties of black carbon at an urban background site in Athens, Greece. Atmos. Environ. 222, 117137.

Li, C.L., Bosch, C., Kang, S.C., Andersson, A., Chen, P.F., Zhang, Q.G., Cong, Z.Y., Chen, B., Qin, D.H., Gustafsson, O., 2016a. Sources of black carbon to the Himalayan-Tibetan Plateau glaciers. Nat. Commun. 7, 12574.

Li, C.L., Yan, F.P., Kang, S.C., Chen, P.F., Hu, Z.F., Gao, S.P., Qu, B., Sillanpaa, M., 2016b. Light absorption characteristics of carbonaceous aerosols in two remote stations of the southern fringe of the Tibetan Plateau, China. Atmos. Environ. 143, 79–85.

Li, C.L., Yan, F.P., Kang, S.C., Yan, C.Q., Hu, Z.F., Chen, P.F., et al., 2020. Carbonaceous matter in the atmosphere and glaciers of the Himalayas and the Tibetan Plateau: An investigative review. Environ. Int. 146, 106281.

Li, S., Zhu, M., Yang, W., Tang, M., Huang, X., Yu, Y., et al., 2018. Filter-based measurement of light absorption by brown carbon in PM2.5 in a megacity in South China. Sci. Total Environ. 633, 1360–1369.

Massabó, D., Caponi, L., Bernardoni, V., Bove, M.C., Brotto, P., Calzolai, G., et al., 2015. Multi-wavelength optical determination of black and brown carbon in atmospheric aerosols. Atmos. Environ. 108, 1–12.

Martinsson, J., Eriksson, A.C., Nielsen, I.E., Malmborg, V.B., Ahlberg, E., Andersen, C., et al., 2015. Impacts of combustion conditions and photochemical processing on the light absorption of biomass combustion aerosol. Environ. Sci. Technol. 49 (24), 14663–14671.

Moschos, V., Kumar, N.K., Daellenbach, K.R., Baltensperger, U., Prévôt, A.S.H., El Haddad, I., 2018. Source apportionment of brown carbon absorption by coupling ultravioletvisible spectroscopy with aerosol mass spectrometry. Environ. Sci. Technol. Lett. 5, 302–308.

Nair, V.S., Babu, S.S., Moorthy, K.K., Sharma, A.K., Marinoni, A., Ajai, 2013. Black carbon aerosols over the Himalayas: direct and surface albedo forcing. Tellus B 65, 19738.

Negi, P.S., Pandey, C.P., Singh, N., 2019. Black carbon aerosols in the ambient air of Gangotri Glacier valley of northwestern Himalaya in India. Atmos. Environ. 214, 116879.

Pandey, C.P., Singh, J., Soni, V.K., Singh, N., 2020. Yearlong first measurements of black carbon in the western Indian Himalaya: Influences of meteorology and fire emissions. Atmos. Pollut. Res. 11, 1199–1210.

Pani, S.K., Wang, S.H., Lin, N.H., Chantara, S., Lee, C.T., Thepnuan, D., 2020. Black carbon over an urban atmosphere in northern peninsular Southeast Asia: Characteristics, source apportionment, and associated health risks. Environ. Pollut. 259, 113871.

Park, S., Son, S.C., Lee, S., 2018. Characterization, sources, and light absorption of fine organic aerosols during summer and winter at an urban site. Atmos. Res. 213, 370–380.

Pathak, R.K., Wang, T., Ho, K.F., Lee, S.C., 2011. Characteristics of summertime PM2.5 organic and elemental carbon in four major Chinese cities: Implications of high acidity for water-soluble organic carbon (WSOC). Atmos. Environ. 45, 318–325.

Pavese, G., Calvello, M., Castagna, J., Esposito, F., 2020. Black carbon and its impact on air quality in two semi-rural sites in Southern Italy near an oil pre-treatment plant. Atmos. Environ. 233, 117532.

Pokhrel, R.P., Beamesderfer, E.R., Wagner, N.L., Langridge, J.M., Lack, D.A., Jayarathne, T., et al., 2017. Relative importance of black carbon, brown carbon, and absorption enhancement from clear coatings in biomass burning emissions. Atmos. Chem. Phys. 17, 5063–5078.

Prabhu, V., Soni, A., Madhwal, S., Gupta, A., Sundriyal, S., Shridhar, V., et al., 2020. Black carbon and biomass burning associated high pollution episodes observed at Doon valley in the foothills of the Himalayas. Atmos. Res. 243, 105001.

Pu, W., Zhao, X., Shi, X., Ma, Z., Zhang, X., Yu, B., 2015. Impact of long-range transport on aerosol properties at a regional background station in Northern China. Atmos. Res. 153, 489–499.

Qin, Y.M., Tan, H.B., Li, Y.J., Li, Z.J., Schurman, M.I., Liu, L., et al., 2018. Chemical characteristics of brown carbon in atmospheric particles at a suburban site near Guangzhou, China. Atmos. Chem. Phys. 18, 16409–16418.

Qiu, X., Duan, L., Gao, J., Wang, S., Chai, F., Hu, J., et al., 2016. Chemical composition and source apportionment of PM10 and PM2.5 in different functional areas of Lanzhou. China. J. Environ. Sci. 40, 75–83.

Qiu, Y., Wu, X., Zhang, Y., Xu, L., Hong, Y., Chen, J., et al., 2019. Aerosol light absorption in a coastal city in Southeast China: Temporal variations and implications for brown carbon. J. Environ. Sci. 80, 257–266.

Rehman, I.H., Ahmed, T., Praveen, P.S., Kar, A., Ramanathan, V., 2011. Black carbon emissions from biomass and fossil fuels in rural India. Atmos. Chem. Phys. 11, 7289–7299.

Rigler, M., Drinovec, L., Lavric, G., Vlachou, A., Prevot, A.S.H., Jaffrezo, J.L., et al., 2020. The new instrument using a TC–BC (total carbon–black carbon) method for the online measurement of carbonaceous aerosols. Atmos. Meas. Tech. 13, 4333–4351.

Saleh, R., Marks, M., Heo, J., Adams, P.J., Donahue, N.M., Robinson, A.L., 2015. Contribution of brown carbon and lensing to the direct radiative effect of carbonaceous aerosols

from biomass and biofuel burning emissions. J. Geophys. Res. 120 10.285-10.296.
Satish, R., Shamjad, P., Thamban, N., Tripathi, S., Rastogi, N., 2017. Temporal characteristics of brown carbon over the Central Indo-Gangetic Plain. Envir. Sci. Technol. 51, 6765–6772.
Segura, S., Estellés, V., Esteve, A.R., Marcos, C.R., Utrillas, M.P., Martínez-Lozano, J.A., 2016. Multiyear in-situ measurements of atmospheric aerosol absorption properties at an urban coastal site in western Mediterranean. Atmos. Environ. 129, 18–26.
Sharma, S.K., Mandal, T.K., Saxena, M., Sharma, R.A., Datta, A., Saud, T., 2014. Variation of OC, EC, WSIC and trace metals of PM10 in Delhi, India. J. Atmos. Sol. Terr. Phys. 113, 10–22.
Shamjad, P.M., Tripathi, S.N., Thamban, N.M., Vreeland, H., 2016. Refractive index and absorption attribution of highly absorbing brown carbon aerosols from an Urban Indian City-Kanpur. Sci. Rep. 6, 37735.
Srinivas, B., Rastogi, N., Sarin, M.M., Singh, A., Singh, D., 2016. Mass absorption efficiency of light absorbing organic aerosols from source region of paddyresidue burning emissions in the Indo-Gangetic Plain. Atmos. Environ. 125, 360–370.
Sun, T.L., Wu, C., Wu, D., Liu, B., Sun, J.Y., Mao, X., et al., 2020. Time-resolved black carbon aerosol vertical distribution measurements using a 356-m meteorological tower in Shenzhen. Theor. Appl. Climatol. 140, 1263–1276.
Taheri, A., Aliasghari, P., Hosseini, V., 2019. Black carbon and PM2.5 monitoring campaign on the roadside and residential urban background sites in the city of Tehran. Atmos. Environ. 218, 116928.
Tan, J.H., Xiang, P., Zhou, X.M., Duan, J.C., Ma, Y.L., He, K.B., et al., 2016. Chemical characterization of humic-like substances (HULIS) in PM2.5 in Lanzhou, China. Sci. Total Environ. 573, 1481–1490.
Tan, J.H., Zhang, L.M., Zhou, X.M., Duan, J.C., Li, Y., Hu, J.N., et al., 2017. Chemical characteristics and source apportionment of PM2.5 in Lanzhou, China. Sci. Total Environ. 601-602, 1743–1752.
Tan, Y., Wang, H.L., Shi, S.S., Shen, L.J., Zhang, C., Zhu, B., et al., 2020. Annual variations of black carbon over the Yangtze River Delta from 2015 to 2018. J. Environ. Sci. 96, 72–84.
Titos, G., Lyamani, H., Cazorla, A., Sorribas, M., Foyo-Moreno, I., Wiedensohler, A., Alados-Arboledas, L., 2014. Study of the relative humidity dependence of aerosol light-scattering in southern Spain. Tellus B 66, 24536.
Turpin, B.J., Lim, H.J., 2001. Species contributions to PM2.5 mass concentrations: revisiting common assumptions for estimating organic mass. Aerosol. Sci. Technol. 35, 602–610.
Wang, J., Nie, W., Cheng, Y., Shen, Y., Chi, X., Wang, J., et al., 2018. Light absorption of brown carbon in eastern China based on 3-year multi-wavelength aerosol optical property observations and an improved absorption Ångström exponent segregation method. Atmos. Chem. Phys. 218, 9061–9074.
Wang, M., Xu, B., Wang, N., Cao, J., Tie, X., Wang, H., et al., 2016a. Two distinct patterns of seasonal variation of airborne black carbon over Tibetan Plateau. Sci. Total Environ. 573, 1041–1052.
Wang, Y.N., Jia, C.H., Tao, J., Zhang, L.M., Liang, X.X., Ma, J.M., et al., 2016b. Chemical characterization and source apportionment of $PM_{2.5}$ in a semi-arid and petrochemical-industrialized city, Northwest China. Sci. Total Environ. 573, 1031–1040.
Washenfelder, R.A., Attwood, A.R., Brock, C.A., Guo, H., Xu, L., Weber, R.J., et al., 2015. Biomass burning dominates brown carbon absorption in the rural southeastern United States. Geophys. Res. Lett. 42, 653–664.
Wei, C., Wang, M.H., Fu, Q.Y., Dai, C., Huang, R., Bao, Q., 2020. Temporal characteristics and potential sources of black carbon in megacity Shanghai, China. J. Geophys. Res 125, e2019JD031827.
Williams, M.A., Kumar, T.V.L., Rao, D.N., 2019. Characterizing black carbon aerosols in relation to atmospheric boundary layer height during wet removal processes over a semi urban location. J. Atmos. Sol-Terr. Phys. 182, 165–176.
Wu, G.M., Ram, K., Fu, P.Q., Wang, W., Zhang, Y.L., Liu, X.Y., et al., 2019. Water-soluble brown carbon in atmospheric aerosols from Godavari (Nepal), a regional representative of South Asia. Environ. Sci. Technol. 53, 3471–3479.
Yan, J., Wang, X., Gong, P., Wang, C., Cong, Z., 2018. Review of brown carbon aerosols: recent progress and perspectives. Sci. Total Environ. 634, 1475–1485.
Yang, M., Howell, S.G., Zhuang, J., Huebert, B.J., 2009. Attribution of aerosol light absorption to black carbon, brown carbon, and dust in China - interpretations of atmospheric measurements during EAST-AIRE. Atmos. Chem. Phys. 9, 2035–2050.
Yuan, J.F., Huang, X.F., Cao, L.M., Cui, J., Zhu, Q., Huang, C.N., et al., 2016. Light absorption of brown carbon aerosol in the PRD region of China. Atmos. Chem. Phys. 16, 1433–1443.
Xia, Y.J., Wu, Y.F., Huang, R.J., Xia, X.A., Tang, J., Wang, M., et al., 2020. Variation in black carbon concentration and aerosol optical properties in Beijing: Role of emission control and meteorological transport variability. Chemosphere 254, 126849.
Xie, C., Xu, W., Wang, J., Wang, Q., Liu, D., Tang, G., et al., 2019. Vertical characterization of aerosol optical properties and brown carbon in winter in urban Beijing, China. Atmos. Chem. Phys. 19, 165–179.
Xiao, S.H., Yu, X.N., Zhu, B., Kumar, K.R., Li, M., Li, L., 2020. Characterization and source apportionment of black carbon aerosol in the Nanjing Jiangbei New Area based on two years of measurements from Aethalometer. J. Aerosol. Sci. 139, 105461.
Zhang, W.Y., Wang, W.G., Li, J., Ma, S.L., Lian, C.F., Li, K., et al., 2021. Light absorption properties and potential sources of brown carbon in Fenwei Plain during winter 2018-2019. J. Environ. Sci. 102, 53–63.
Zhang, X., Li, Z.Q., Wang, F.T., Song, M.Y., Zhou, X., Ming, J., 2020b. Carbonaceous aerosols in PM1, PM2.5, and PM10 size fractions over the Lanzhou City, Northwest China. Atmosphere 11, 1368.
Zhang, X., Lin, Y.H., Surratt, J.D., Zotter, P., Prévôt, A.S.H., Weber, R.J., 2011. Light absorbing soluble organic aerosol in Los Angeles and Atlanta: a contrast in secondary organic aerosol. Geophys. Res. Lett. 38, 2–5.
Zhang, X., Li, Z.Q., Ming, J., Wang, F.T., 2020a. One-year measurements of equivalent black carbon, optical properties, and sources in the urumqi river Valley, Tien Shan, China. Atmosphere 11, 478.
Zhang, Y., Li, M., Bravo, M.A., Jin, L., Nori-Sarma, A., Xu, Y., et al., 2014. Air Quality in Lanzhou, a Major Industrial City in China: Characteristics of Air Pollution and Review of Existing Evidence from Air Pollution and Health Studies. Water Air Soil Pollut. 225, 2187.
Zhang, Y.L., Kang, S.C., 2018. Characteristics of carbonaceous aerosols analyzed using a multiwavelength thermal/optical carbon analyzer: A case study in Lanzhou City. Sci. China. Earth. Sci. 61, 389–402.
Zhao, R., Lee, A.K.Y., Huang, L., Li, X., Yang, F., Abbatt, J.P.D., 2015. Photochemical processing of aqueous atmospheric brown carbon. Atmos. Chem. Phys. 15, 6087–6100.
Zhao, Z., Wang, Q., Xu, B., Shen, Z., Huang, R., Zhu, C., et al., 2017. Black carbon aerosol and its radiative impact at a high-altitude remote site on the southeastern Tibet Plateau. J. Geophys. Res: Atmos. 122, 5515–5530.
Zheng, H., Kong, S., Zheng, M., Yan, Y., Yao, L., Zheng, S., et al., 2020. A 5.5-year observations of black carbon aerosol at a megacity in Central China: Levels, sources, and variation trends. Atmos. Environ. 232, 117581.
Zhao, S.P., Yu, Y., Yin, D.Y., Qin, D.H., Yu, Z.S., Dong, L.X., et al., 2019. PM1 carbonaceous aerosols during winter in a typical valley city of western China: vertical profiles and the key influencing factors. Atmos. Environ. 202, 75–92.